Timing Jitter and Intensity Noise Characterization of a 122-MHz All-PM NALM Mode-Locked Fiber Laser

Yihan Pi, Haochen Tian, Runmin Li, Yan Han, Youjian Song, *Senior Member, IEEE*, and Minglie Hu

***Abstract*— Mode-locked lasers with low noise performance, such as low timing jitter and relative intensity noise are essential for high-precision applications. In this letter, we demonstrated a 122-MHz all-polarization-maintaining mode-locked Er-doped fiber laser based on a nonlinear amplifying loop mirror. A hybrid component integrating a wavelength division multiplexer and a phase shifter is applied to increase the repetition rate. The relative intensity noise is 0.004% and 0.76% rms (integrated from 1 MHz to 100 Hz) from two output ports. The timing jitter characteristic is measured by the delayed optical heterodyne method. The timing jitter is ∼1.9 fs rms (integrated from 1 MHz to 10 Hz) of both two output ports. The origin of the timing jitter of this laser is analyzed numerically based on the well-established theoretical model using the laser's repetition rate, cavity dispersion, etc.**

***Index Terms*— Mode-locked fiber laser, nonlinear amplifying loop mirror, all-polarization-maintaining, timing jitter.**

I. Introduction

FIBER mode-locked lasers become ideal reliable ultrashort optical pulse sources due to their compactness, low cost and robustness. In the meanwhile, noise performance of the mode-locked fiber lasers also has been systematically studied. Consequently, low-noise mode-locked fiber lasers enable advances in high-precision time-frequency applications [1]–[4].

Nonlinear amplifying loop mirror (NALM)-based lasers, which can be applied in all-PM configuration, have shown superior performance in robustness, long-term stability as well as self-starting operation [5]–[8]. In particular, a NALM loop and a linear arm are desirable for shorter cavity lengths, enabling higher repetition rates. In 2016, Hänsel *et al.* presented a 250 MHz mode-locked all-PM-fiber Er-fiber laser based on NALM [8]. This laser structure could be implemented to Er-doped [7]–[10], Yb-doped [8], [11], [12], Tm-doped [8] fiber, and other rare-earth-doped fiber. However, the typical repetition rate achieved in this scheme ranges from 30 MHz to 90 MHz. The major difficulty of building an all-PM NALM mode-locked fiber laser with repetition rate above 100 MHz is the integration of the fiber components. A 121-MHz all-PM NALM-based fiber laser with an integrated non-reciprocal phase shifter was reported by Yin *et al.* [13]. A recent work by Deng *et al.* shows a 201-MHz NALM Er-doped fiber laser using a hybrid component involving a wavelength division multiplexer (WDM), a phase shifter, and an optical coupler with a 40:60 splitting ratio [14]. These designs of all-PM-fiber laser configuration simplify the laser configuration, enhance laser stability and thus enable their applications in some harsh environments.

On the other side, detailed studies and optimization of the laser's intrinsic noise characteristics, such as intensity noise and timing jitter are particularly important for the operation of low-noise mode-locked fiber lasers and their further advances in high-precision applications. Balanced optical cross correlation (BOC) and optical heterodyne were proposed to achieve attosecond- or even yoctosecond-resolution timing jitter characterization [15], [16]. Two repetition-rate-matched lasers are generally required while applying these methods. Therefore a reference-free high-resolution method has been proposed based on the delayed optical heterodyne (DOH) technique [17]–[19]. In this method, a long fiber delay line (FDL) and an acoustic optical frequency shifter (AOFS) are used to create an artificial reference laser with a certain frequency offset from the under-test laser. Consequently, this method is particularly desirable when two identical mode-locked lasers are not available.

In this letter, we demonstrated an all-PM NALM-based mode-locked laser. An integrated device combining the WDM and non-reciprocal phase shifter was placed in the NALM loop to shorten the cavity length. The pulse repetition rate was 122.1 MHz. In addition, we measured and compared the relative intensity noise (RIN) and the timing jitter of two output ports in the demonstrated laser. The origin of the dominant noise source was analyzed through comparing our measurement results with the well-established Paschotta's theoretical model [20]. The noise measurement and analysis are significant for intrinsic noise optimization of the lasers, paving

Manuscript received October 7, 2021; revised October 26, 2021; accepted November 1, 2021. Date of publication November 8, 2021; date of current version November 17, 2021. This work was supported by the National Natural Science Foundation of China under Grant 61975144 and Grant 61827821. *(Corresponding author: Haochen Tian.)*

Yihan Pi, Haochen Tian, Runmin Li, Youjian Song, and Minglie Hu are with the Ultrafast Laser Laboratory, Key Laboratory of Opto-electronic Information Science and Technology of Ministry of Education, School of Precision Instruments and Opto-electronics Engineering, Tianjin University, Tianjin 300072, China (e-mail: haochentian@tju.edu.cn).

Yan Han is with the Ultrafast Laser Laboratory, Key Laboratory of Opto-electronic Information Science and Technology of Ministry of Education, School of Precision Instruments and Opto-electronics Engineering, Tianjin University, Tianjin 300072, China, and also with the College of Physics and Optoelectronics, Taiyuan University of Technology, Taiyuan 030024, China.

Color versions of one or more figures in this letter are available at https://doi.org/10.1109/LPT.2021.3125994.

Digital Object Identifier 10.1109/LPT.2021.3125994

1041-1135 © 2021 IEEE. Personal use is permitted, but republication/redistribution requires IEEE permission.
See https://www.ieee.org/publications/rights/index.html for more information.

Authorized licensed use limited to: TIANJIN UNIVERSITY. Downloaded on November 30,2021 at 08:11:03 UTC from IEEE Xplore. Restrictions apply.

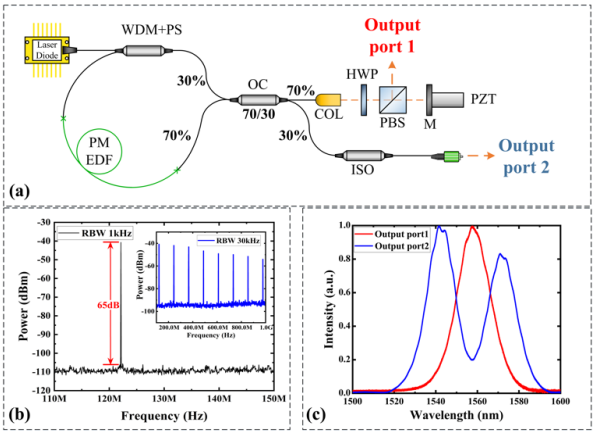

Fig. 1. (a) Schematic of the all-PM NALM-based fiber laser. WDM, wavelength division multiplexer; PS, phase shifter; PM-EDF, polarization-maintaining Er-doped fiber; OC, optical fiber coupler; COL, collimator; HWP, half-wave plate; PBS, polarization beam splitter; M, reflective mirror; PZT, piezoelectric; ISO, isolator. (b) RF spectra of the laser. (c) Optical spectra of output pulses from the two ports.

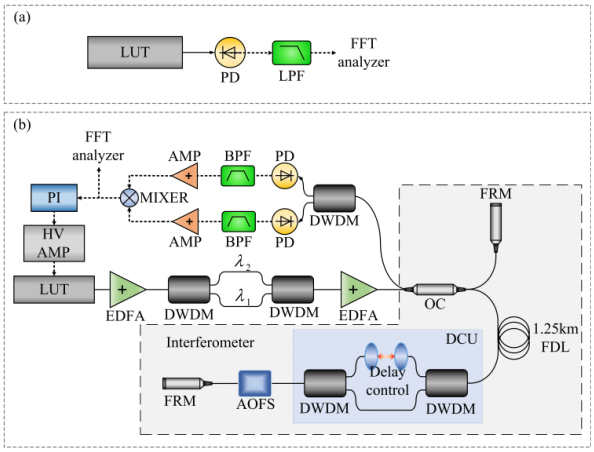

Fig. 2. Experimental setup. (a) RIN measurement setup. LUT, laser under test; PD, photodetector; LPF, low-pass filter. (b) Timing jitter measurement setup based on delayed optical heterodyne technique. EDFA, Er-doped fiber amplifier; DWDM, dense wavelength division multiplexer; OC, optical fiber coupler; FRM, Faraday rotating mirror; FDL, dispersion-compensated fiber delay line; DCU, delay control unit; AOFS, acousto-optic frequency shifter; BPF, bandpass filter; AMP, amplifier; PI, proportional-integral servo; HV AMP, high-voltage amplifier.

the way for the operation of low-noise optical frequency comb.

II. Experimental Setup

Fig.1(a) illustrates the schematic of the all-PM NALM-based fiber laser. The laser was composed of a NALM loop and a linear arm. The NALM loop contained a 2 × 2 PM optical fiber coupler (OC) with 70:30 splitting ratio, a 0.5-m PM Er-doped fiber (nLight Liekki, Er80-4/125-HD-PM), a 976/1550 nm PM WDM with fast axis blocked, and a non-reciprocal phase shifter (PS) providing a 0.5-π linear phase bias for self-started mode-locking. In order to shorten the cavity length and achieve a higher repetition rate, we applied a hybrid WDM-PS instead of two separate devices. The gain fiber with group velocity dispersion (GVD) of 0.02804 ps^2/m at 1550 nm was placed asymmetrically in the loop and pumped by a single-mode 976 nm laser diode (LD) through the WDM-PS. The WDM-PS and EDF were fiber-fused between two ports at same end of the OC. The 70% port at the other end of the OC was regarded as the reflection arm of NALM and connected to the linear arm, which comprised a fiber collimator (COL) and a reflective mirror (M). A polarization beam splitter cube (PBS) and a half-wave plate (HWP) were inserted between COL and M to couple out a part of the beam, which was the laser Output port 1. The output coupling ratio and intra-cavity loss could be adjusted by finely tuning HWP. The other port of the OC was regarded as the transmission arm of NALM and was used as Output port 2. All of the fibers in the cavity were PM fibers, aiming to increase the mode-locking stability and robustness. The overall fiber length in the cavity was ∼1.58 m. The estimated net cavity dispersion was -0.0107 ps^2 at 1550nm.

The mode-locking operation could be initiated at 965 mW pump in the multi-pulsing regime. Then we decreased the pump power to obtain a single-pulse state. The pump power for maintaining stable single-pulse operation ranged from 350 mW to 400 mW. At 400 mW pump power, the average power from port 1 and port 2 were 5.96 mW and 9.02 mW, respectively.

We then measured the repetition rate's radio-frequency spectrum of the demonstrated laser via an InGaAs photodetector (Thorlabs, DET01CFC/M) and an RF spectrum analyzer (RIGOL, RSA3030). As shown in Fig. 1(b), the repetition rate of the laser was 122.1 MHz, with 65 dB signal-to-noise ratio (SNR) of the fundamental frequency at 1 kHz resolution bandwidth (RBW). Fig. 1(c) shows the optical spectrum of the laser with 0.02 nm resolution measured by an optical spectrum analyzer (Yokogawa, AQ6370B). The full-width-half-maximum (FWHM) bandwidth were 19 nm and 43 nm at a 1557 nm center wavelength for Output port 1 and port 2. The corresponding transform-limited pulse durations were 157 fs and 108 fs, respectively. Note that the spectra of these two ports were in different shapes, because the Output port 1 and the Output port 2 correspond to the reflected and transmitted beam by the NALM, respectively.

III. Experimental Results

A. Relative Intensity Noise (RIN) Measurement

Fig. 2(a) shows the schematic of the RIN measurement setup. The optical pulses from the laser under-test were detected by an InGaAs switchable-gain-amplified photodetector (Thorlabs, PDA20CS-EC). The bandwidth was 10 MHz. The signal from the photodetector was filtered by a low pass filter (DC to 1.9 MHz) and then sent to a FFT analyzer (SRS, SR770).

The RIN power spectral density (PSD) of the NALM-based laser could be retrieved from the voltage PSD measured by the FFT analyzer, as represented in Fig. 3. The blue curve and the red curve correspond to the RIN PSD of the optical pulses from Output port 2 and Output port 1, respectively. The integrated value of RIN of pulses from Output port 1 and port 2 were 0.004% and 0.76% (integrated from 1 MHz to 100 Hz), respectively. Above 100 kHz offset frequency, RIN measurement was limited by the noise floor of the photodetector.

Authorized licensed use limited to: TIANJIN UNIVERSITY. Downloaded on November 30,2021 at 08:11:03 UTC from IEEE Xplore. Restrictions apply.

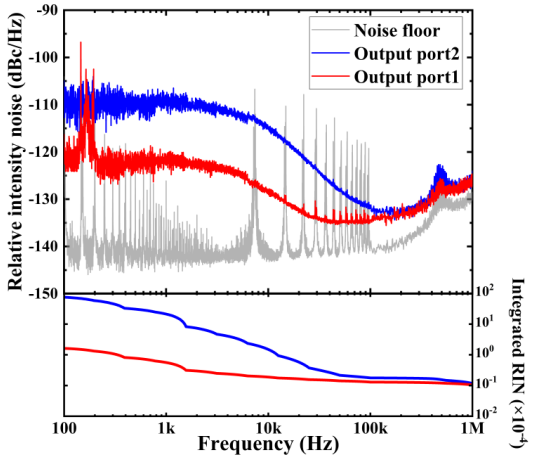

Fig. 3. RIN PSD of the optical pulses from Output port 1 and Output port 2 from the NALM-based laser.

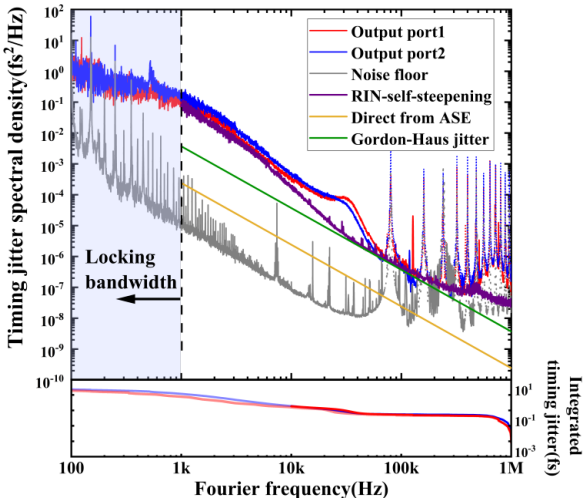

Fig. 4. Timing jitter measurement results and the integrated timing jitter. Calculated timing jitter resulting from direct-coupled jitter from ASE (orange curve), Gorden-Haus jitter (green curve), and RIN coupled jitter by self-steepening effect (purple curve).

Interesting differences could be observed between the two Output ports. Compared to port 1, the RIN of Output port 2 is 10 dB higher from 100 Hz to 10 kHz. This could be explained by the large amounts of amplified spontaneous emission (ASE) noise and pump LD technical noise directly coupling from the NALM to the Output port 2. In addition, the limited bandwidth (typically $\sim$ 40 nm) of intracavity fiber devices could lead to lower RIN level of pulses from Output port 1 due to filter effects [21].

B. Timing Jitter Measurement

In addition to RIN measurement, we also characterized the timing jitter of the NALM-based laser. The setup of timing jitter measurement based on DOH is shown in Fig. 2(b). The laser under-test was designed with an intra-cavity piezo-actuated mirror, as shown in Fig. 1(a), for the low-bandwidth cavity length tuning. The output pulse train was amplified by a home-built EDFA, and then sent to a pair of dense wavelength division multiplexers (DWDMs) to filter out two wavelength components at $\lambda_1 = 1537$ nm and $\lambda_2 = 1566$ nm within $\sim$1.6 nm (200 GHz) bandwidth. Another EDFA amplified the filtered pulse train to 20 mW before entering into the asymmetric fiber Michelson interferometer.

A 2×2 optical fiber coupler in the interferometer split the optical pulse trains into the reference arm and delayed arm. Faraday rotating mirrors (FRMs) were placed at the end of both arms to reflect the pulses. In the delayed arm, the optical pulses went through a 1.25-km long dispersion-compensated fiber delay line (FDL), a delay control unit (DCU), and an acousto-optic frequency shifter (AOFS). The optical path difference between two wavelength segments, which was introduced by the dispersion of the 1.25-km long fiber, could be compensated by finely adjusting the fiber delay in the DCU. The AOFS was utilized to shift the optical signals at the modulation frequency $f_{mod} = 50$ MHz. Since each pulse train would pass through the AOFS twice, the pulses in the delayed arm had $2f_{mod} = 100$ MHz frequency offset compared with the pulses in the reference arm. At the output arm of the interferometer, λ_1 and λ_2 were split, and then the heterodyne beat notes of both wavelength components were detected by two separate PDs. Each beat note carried the frequency noise ($\delta[\tau(mf_{rep} + f_{ceo} + 2f_{mod})]$ for λ_1 and $\delta[\tau(nf_{rep} + f_{ceo} + 2f_{mod})]$ for λ_2), where f_{rep} and f_{ceo} represent repetition-rate frequency and carrier-envelope-offset frequency, respectively, and τ is the round-trip delay time between the two arms of the interferometer. The error signal containing the repetition rate frequency noise $\delta\tau(m\text{-}n)f_{rep}$ could be obtained via mixing the two beat notes in a frequency mixer. In this way, the common noise term, $(f_{ceo} + 2f_{mod})$ was rejected. In order to maintain the error signal at the linear range of discrimination slope, low-bandwidth phase locking was demanded. The error signal from the mixer was amplified by a high-voltage amplifier and then used to control to the intra-cavity PZT through a proportional-integral servo (PI) (Newfocus, LB1005). Thus the laser's repetition rate was stabilized to the FDL. At last, voltage noise PSD was measured by an FFT analyzer.

A transfer function $T(f) = V_{peak}[(1\text{-}\exp(\text{-}i \times 2\pi\tau))/(i \times f)]$ [V/Hz] was used to convert the measured voltage noise PSD to the frequency noise PSD of $(m\text{-}n)f_{rep}$, where V_{peak} is the amplitude of the low-pass filtered mixer output voltage from the interference pattern, f is the Fourier frequency. Finally, the frequency noise of $(m\text{-}n)f_{rep}$ was converted to timing jitter and plotted in Fig. 4. Moreover, the transfer function has nulls for Fourier frequency at $1/\tau$ (i.e. $\sim$80 kHz in this experiment) and its harmonics, which means that the detection is nullified at these frequencies [19].

The timing jitter PSD result of the NALM-based laser is plotted in Fig. 4. Note that the measurement resolution is $\sim 10^{-7}$ fs^2/Hz level at 100 kHz offset frequency. The artifact spikes (at $\sim$80 kHz and its harmonics) represented by dotted curves were induced by the sensitivity null points of the FDL, not the natural frequency noise peaks of the tested laser. The corresponding timing jitter integrated from 1 MHz to 1 kHz were 1.85 fs and 1.91 fs for Output port 1 and port 2, respectively. When integrating the timing jitter PSD curve, the artifact peaks at sensitivity null points were simply removed. As shown in Fig. 4, the two output ports' timing jitter PSD spectra were basically similar.

Authorized licensed use limited to: TIANJIN UNIVERSITY. Downloaded on November 30,2021 at 08:11:03 UTC from IEEE Xplore. Restrictions apply.

The fundamental limit of timing jitter at high frequency offset (typically > 10 kHz) in mode-locked laser is determined by ASE quantum noise. There are two ways for ASE quantum noise to couple to timing jitter. First, the ASE quantum noise can have direct influence on timing jitter in the time domain, resulting in a $1/f^2$ slope of timing jitter spectral density. Second, the ASE noise can also induce timing jitter indirectly by causing the center frequency fluctuation via intra-cavity group delay dispersion (GVD), which is named Gordon–Haus jitter. In this case, the timing jitter spectral density shows a $1/f^2$ slope at low offset frequency range (<10 MHz in this calculation) and a $1/f^4$ slope at high offset frequency range (>10 MHz in this calculation). Besides the fundamental limit, other technique noise, such as intensity noise, can also be coupled in timing jitter through self-steepening effect, particularly in fiber mode-locked lasers [22]. The numerical analysis based on well-established Paschotta's theoretical model was used here to calculate the projected timing jitter PSD from three different effects: directly coupled from ASE, Gordon–Haus jitter, and RIN-coupled jitter by self-steepening effect [18], [20]. The laser parameters used here were: 122-MHz repetition rate, -0.0107 ps^2 net intra-cavity dispersion, 1557 nm center wavelength, and 157-fs FWHM pulse width. The saturated gain was 0.69 calculated from a round-trip cavity loss of 50%. Intra-cavity pulse energy was 0.26 nJ. It should be note that, the RIN data from Output port 1 was used for calculation, due to the reason that this reflects the intensity fluctuation of the pulses circulating in the cavity. As plotted in Fig. 4, the RIN-coupled timing jitter by self-steepening effect is dominant in this laser for Fourier frequency between 1 kHz and 10 kHz. However, in the Fourier frequency range from 60 kHz to 100 kHz, Gordon–Haus jitter played the most important role.

IV. Conclusion

In summary, we have presented an all-PM NALM-based fiber laser with 122-MHz repetition rate. The RIN and timing jitter have been measured and analyzed. We have also noted that the RIN spectrum shows markedly different levels from two separate output ports from the same laser. The integrated RIN are 0.004% and 0.76 % (from 1 MHz to 100 Hz). By contrast, the timing jitter spectra are almost identical, resulting in ~1.9 fs integrated timing jitter (integrated from 1 MHz to 10 kHz). Pulse trains with distinct RIN PSDs but with similar timing jitter PSDs from one laser cavity was also reported in Ref [21]. The demonstrated laser could be built without spatial parts (the PBS, the mirror and PZT in the linear arm), resulting an integrated, compact, all-PM-fiber configuration, which can be utilized as a reliable, flexible, and robust ultrafast fiber laser source. The noise measurement and analysis set foundation for intrinsic noise optimization of the lasers, paving the way for their further operation of low-noise optical frequency comb.

References

[1] S. A. Diddams, K. Vahala, and T. Udem, "Optical frequency combs: Coherently uniting the electromagnetic spectrum," *Science*, vol. 369, no. 6501, p. 3676, Jul. 2020, doi: 10.1126/science.aay3676.

[2] I. Coddington, W. C. Swann, L. Nenadovic, and N. R. Newbury, "Rapid and precise absolute distance measurements at long range," *Nature Photon.*, vol. 3, pp. 351–356, May 2009, doi: 10.1038/nphoton.2009.94.

[3] N. Picqué and T. W. Hänsch, "Frequency comb spectroscopy," *Nature Photon.*, vol. 13, no. 3, pp. 146–157, 2019, doi: 10.1038/s41566-018-0347-5.

[4] R. Liao, H. Tian, W. Liu, R. Li, Y. Song, and M. Hu, "Dual-comb generation from a single laser source: Principles and spectroscopic applications towards mid-IR—A review," *J. Phys., Photon.*, vol. 2, no. 4, Sep. 2020, Art. no. 042006, doi: 10.1088/2515-7647/aba66e.

[5] R. Li *et al.*, "All-polarization-maintaining dual-wavelength mode-locked fiber laser based on Sagnac loop filter," *Opt. Exp.*, vol. 26, no. 22, p. 28302, Oct. 2018, doi: 10.1364/OE.26.028302.

[6] C. Aguergaray, N. G. R. Broderick, M. Erkintalo, J. S. Y. Chen, and V. Kruglov, "Mode-locked femtosecond all-normal all-PM Yb-doped fiber laser using a nonlinear amplifying loop mirror," *Opt. Exp.*, vol. 20, no. 10, p. 10545, May 2012, doi: 10.1364/OE.20.010545.

[7] N. Kuse, J. Jiang, C.-C. Lee, T. R. Schibli, and M. E. Fermann, "All polarization-maintaining Er fiber-based optical frequency combs with nonlinear amplifying loop mirror," *Opt. Exp.*, vol. 24, no. 3, p. 3095, Feb. 2016, doi: 10.1364/OE.24.003095.

[8] W. Hänsel *et al.*, "All polarization-maintaining fiber laser architecture for robust femtosecond pulse generation," *Appl. Phys. B, Lasers Opt.*, vol. 123, no. 1, p. 44, Jan. 2017, doi: 10.1007/s00340-016-6598-2.

[9] J. Zhou, W. Pan, X. Fu, L. Zhang, and Y. Feng, "Environmentally-stable 50-fs pulse generation directly from an Er: Fiber oscillator," *Opt. Fiber Technol.*, vol. 52, Nov. 2019, Art. no. 101963, doi: 10.1016/j.yofte.2019.101963.

[10] X. Liu *et al.*, "An all polarization-maintaining fiber laser mode locked by nonlinear amplifying loop mirror with different biases," *Laser Phys.*, vol. 30, no. 8, Aug. 2020, Art. no. 085104, doi: 10.1088/1555-6611/ab964b.

[11] Y. Ma *et al.*, "Compact, all-PM fiber integrated and alignment-free ultrafast Yb: Fiber NALM laser with sub-femtosecond timing jitter," *J. Lightw. Technol.*, vol. 39, no. 13, pp. 4431–4438, Mar. 31, 2021, doi: 10.1109/JLT.2021.3070208.

[12] A. S. Mayer *et al.*, "Flexible all-PM NALM Yb: Fiber laser design for frequency comb applications: Operation regimes and their noise properties," *Opt. Exp.*, vol. 28, no. 13, p. 18946, Jun. 2020, doi: 10.1364/OE.394543.

[13] K. Yin, Y.-M. Li, Y.-B. Wang, X. Zheng, and T. Jiang, "Self-starting all-fiber PM Er: Laser mode locked by a biased nonlinear amplifying loop mirror," *Chin. Phys. B*, vol. 28, no. 12, Nov. 2019, Art. no. 124203, doi: 10.1088/1674-1056/ab4d42.

[14] Q. Deng, K. Yin, J. Zhang, X. Zheng, and T. Jiang, "A 200 MHz compact environmentally-stable mode-locked figure-9 fiber laser," *IEEE Photon. J.*, vol. 13, no. 4, Jul. 2021, Art. no. 1500605, doi: 10.1109/JPHOT.2021.3095159.

[15] T. R. Schibli *et al.*, "Attosecond active synchronization of passively mode-locked lasers by balanced cross correlation," *Opt. Lett.*, vol. 28, no. 11, pp. 947–949, 2003, doi: 10.1364/OL.28.000947.

[16] D. Hou, C. C. Lee, Z. Yang, and T. R. Schibli, "Timing jitter characterization of mode-locked lasers with <1 zs/$\sqrt{}$pHz resolution using a simple optical heterodyne technique," *Opt. Lett.*, vol. 40, no. 13, pp. 2985–2988, Jul. 2015, doi: 10.1364/OL.40.002985.

[17] D. Kwon *et al.*, "Reference-free, high-resolution measurement method of timing jitter spectra of optical frequency combs," *Sci. Rep.*, vol. 7, no. 1, p. 40917, Jan. 2017, doi: 10.1038/srep40917.

[18] H. Tian *et al.*, "Optical frequency comb noise spectra analysis using an asymmetric fiber delay line interferometer," *Opt. Exp.*, vol. 28, no. 7, p. 9232, Mar. 2020, doi: 10.1364/OE.386231.

[19] H. Tian *et al.*, "Optical frequency comb stabilized to a fiber delay line," *Appl. Phys. Lett.*, vol. 119, no. 12, Sep. 2021, Art. no. 121106, doi: 10.1063/5.0062785.

[20] R. Paschotta, "Noise of mode-locked lasers (Part II): Timing jitter and other fluctuations," *Appl. Phys. B, Lasers Opt.*, vol. 79, no. 2, pp. 163–173, 2004, doi: 10.1007/s00340-004-1548-9.

[21] D. Kim, D. Kwon, B. Lee, and J. Kim, "Polarization-maintaining nonlinear-amplifying-loop-mirror mode-locked fiber laser based on a 3×3 coupler," *Opt. Lett.*, vol. 44, no. 5, pp. 1068–1071, Feb. 2019, doi: 10.1364/OL.44.001068.

[22] H. Tian, Y. Song, and M. Hu, "Noise measurement and reduction in mode-locked lasers: Fundamentals for low-noise optical frequency combs," *Appl. Sci.*, vol. 11, no. 16, p. 7650, Aug. 2021, doi: 10.3390/app11167650.

Authorized licensed use limited to: TIANJIN UNIVERSITY. Downloaded on November 30,2021 at 08:11:03 UTC from IEEE Xplore. Restrictions apply.